Flexible and Printed Electronics

PAPER • OPEN ACCESS

Laser sintering of copper conductive traces on primer pre-treated additive manufactured 3D surfaces

To cite this article: Ejvind Olsen and Ludger Overmeyer 2021 *Flex. Print. Electron.* **6** 015006

View the article online for updates and enhancements.

You may also like

- Sputtered Au–Ta films with tunable electrical resistivity
L B Bayu Aji, A M Engwall, J H Bae et al.
- Quench and self-protecting behaviour of an intra-layer no-insulation (LNI) REBCO coil at 31.4 T
Y Suetomi, T Yoshida, S Takahashi et al.
- Electrical resistivity and wave character of free electrons in amorphous and nanoglass $Sc_{75}Fe_{25}$
M Ghafari, W D Hutchison, S J Campbell et al.

This content was downloaded from IP address 89.245.22.245 on 14/11/2023 at 08:00

IOP Publishing Flex. Print. Electron. 6 (2021) 015006 https://doi.org/10.1088/2058-8585/abdbfd

Flexible and Printed Electronics

OPEN ACCESS

RECEIVED
31 July 2020

REVISED
21 December 2020

ACCEPTED FOR PUBLICATION
14 January 2021

PUBLISHED
9 February 2021

Original content from this work may be used under the terms of the Creative Commons Attribution 4.0 licence.

Any further distribution of this work must maintain attribution to the author(s) and the title of the work, journal citation and DOI.

PAPER

Laser sintering of copper conductive traces on primer pre-treated additive manufactured 3D surfaces

Ejvind Olsen and Ludger Overmeyer

Institute of Transport and Automation Technology, Leibniz University Hanover, An der Universität 2, Garbsen 30823, Germany

E-mail: ejvind.olsen@ita.uni-hannover.de

Keywords: additive manufacturing, epoxy primer, copper ink, laser curing, 3D conductive traces

Abstract

This paper introduces a novel process for creating conductive copper traces on 3D surfaces from different additive manufacturing technologies by employing printed electronics techniques. An essential step in this process was the dip-coating pre-treatment with a primer to reduce the surface roughness below 100 nm, seal pores if present, and increase the thermal stability. This was followed by a dip-coating with copper nanoparticle ink, drying using a heat gun and thermal curing by laser sintering. The experiments determined the optimal laser peak intensity for achieving conductors with the lowest electrical resistance possible. The laser parameters' processing window provided conductive traces on 3D surfaces with properties comparable to photonic sintering on planar substrates. Thereby, the conductive traces reached electrical specific resistances lower than 18 $\mu\Omega$ cm (elemental copper: $\rho = 1.8$ $\mu\Omega$ cm) and a copper material percentage higher than 90 atom %. Shear tests validated the assembly with surfacemount device (SMD) resistors. Electrical tests resulted in maximum current densities higher than 100 A mm^{-2} and lateral breakdown voltages higher than 2kV mm^{-1}. Thus, this paper presents essential prerequisites for a future application of the technology.

1. Introduction

Electronic circuits' integration into additive manufacturing processes has recently received increased attention for rapid prototyping and unique product design of hybrid electromechanical components. Existing approaches are direct 3D printing of fully conductive material composites [1], the transfer of conductive patterns with hydro printing [2], conductive printing filaments [3], 3D inkjet printing [4] and laser directed structuring-compatible 3D printing materials [5, 6]. New approaches are available through the direct application of printed electronics techniques on additive manufactured surfaces [7].

Printed electronics techniques already have wide applications on planar substrates. They base on either the sequential (inkjet or aerosol jet) or simultaneous (roll to roll or dip coating) ink deposition techniques. After ink deposition, a moderate amount of heat convection or infrared radiation ensures proper drying. Next follows applying high peak temperatures for a short time to sinter the metal particles together with sequential (electrical or laser) or simultaneous (thermal or photonic with flash lamp) processes. Nowadays, printed conductive traces are present in 2D orientated technologies for substrate materials like glass, PET and paper [8].

The application of high viscose metal inks on additive manufactured surfaces has already been investigated in 3D-printer nozzles [9] and aerosol jet processes [10]. This study aims to print on additive manufactured 3D surfaces by dip-coating the circuit carrier in low viscose (2.3×10^{-2} Pas at 25 °C) metal nanoparticles containing ink and subsequent laser sintering. This process has already been extensively studied and applied on 2D surfaces [11–14]. However, high surface roughness, porosity, and polymers' low thermal stability impede the transfer to additive manufactured 3D surfaces. This study investigates the process with different additive manufactured 3D substrates produced with the fused deposition modeling (FDM), multi-jet modeling (MJM), stereolithography apparatus (SLA) and selective laser sintering (SLS) techniques. The different substrate materials are acrylonitrile butadiene styrene (ABS), photopolymer, ceramic-filled epoxy and polypropylene. Preliminary investigations on the bare 3D substrate surfaces from this study show that due to the

© 2021 The Author(s). Published by IOP Publishing Ltd

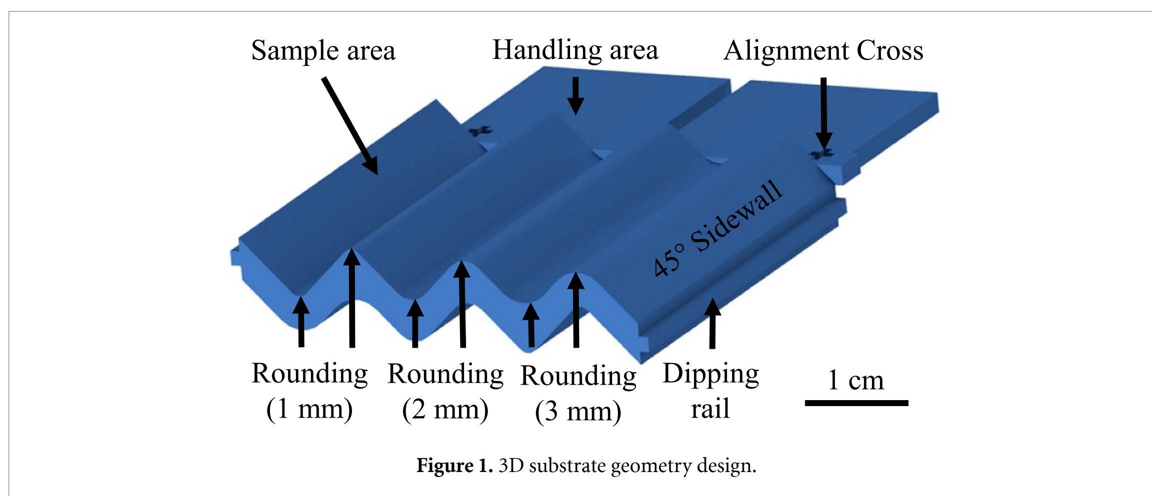

Figure 1. 3D substrate geometry design.

high roughness and low temperature-stability, it is impossible to print conductive traces with low viscose inks directly onto the investigated substrates. The temperature for laser sintering of nanoparticle copper is well below the bulk melting temperature of copper (1085 °C) but still high enough (to 230 °C–420 °C, depending on the particle size) to impede the direct laser sintering of copper traces on top of low-temperature resistant polymer substrates [15, 16]. Hence, this research investigates the pre-treatments of 3D surfaces. Possible pre-treatment options are grinding, (laser) polishing and applying an epoxy-based primer. Priming can simultaneously resolve the issues of non-uniform surface roughness, porosity and thermal stability. That allows employing the process to different additive manufacturing processes (FDM, MJM, SLA and SLS) with the consecutive printing of conductive traces.

2. Approach

2.1. Additive manufactured substrates

The substrate design considers specific demands for optimizing the dip coating and laser process. It has a wave-shaped geometry with 45° sidewall surfaces connected by various rounded areas (3× convex and 3× concave with 1 mm, 2 mm, 3 mm radii), as shown in figure 1.

The 3D substrate includes alignment marks on the handling area, which are necessary to reference the 3D scanner laser system for sintering. The dipping rails enable a reproducible dipping process. Table 1 includes the substrate additive manufacturing details and the initial surface roughness measured with a confocal microscope.

The roughness of additive manufactured 3D surfaces is not homogeneous. The given roughness values represent the highest average measured value on the respective additive manufactured 3D surfaces with different orientations.

2.2. Process structure

The presented production process consists of four main steps:

(a) Additive manufacturing of the circuit carrier
(b) Primer pre-treatment by dip-coating
(c) Dip-coating with copper ink
(d) Laser sintering to produce conductive traces

Figure 2 visualizes the process flow in a 3D scheme without showing the additive manufacturing and laser sintering process.

The dipping station (3D printed) minimizes the amount of ink or primer used in the dipping bath. Rails on the substrate and guide slots of the dipping station prohibit the substrate from touching the dipping station walls and maintain a vertical orientation during the dipping process. In process step number four, a focused laser spot follows the 3D geometry, cures the ink sequentially to fuse the copper ink particles and creates conductive traces. Figure 3 visualizes a detailed process scheme for the laser sintering process.

The straight track is for the laser parametrization on a statistical basis. The meandering structure validates the developed process with a more complex circuit geometry.

2.3. Experiment description

This research compares various printing methods and printing materials regarding their suitability for the introduced primer pre-treatment and the following copper coating and laser sintering process. After manufacturing the circuit carrier and removing supporting material, water and isopropanol treatments clean the parts. A UV hardening epoxy-based liquid primer is wetted by dip-coating and cured under a UV lamp (BlueWave 50 UV). The dip-coating process consists of a 5 s break inside the bath and a dipping speed of 1.5 cm s^{-1}. The dipping process repeats twice before curing with UV light to ensure that the

Table 1. Details of additive manufactured substrates.

Process	Material	Printer	Ra in μm	Rz in μm
FDM	ABS	Creatr HS (Leapfrog)	6,8	42,4
MJM	Photopolymer vero blue	Enden260 VS (Stratasys)	2,0	10,3
SLA	Ceramic filled epoxy resin	SLA 5000 (3D Systems)	1,85	10,8
SLS	Polypropylene	P3 (EOS)	17	94,8

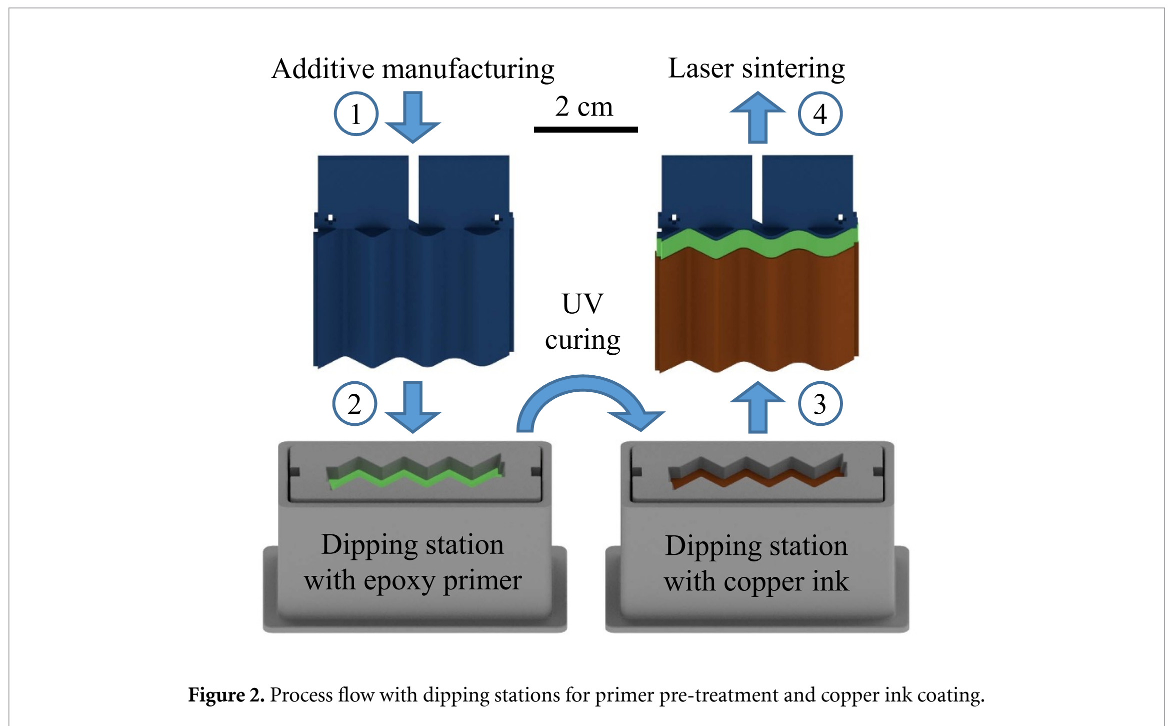

Figure 2. Process flow with dipping stations for primer pre-treatment and copper ink coating.

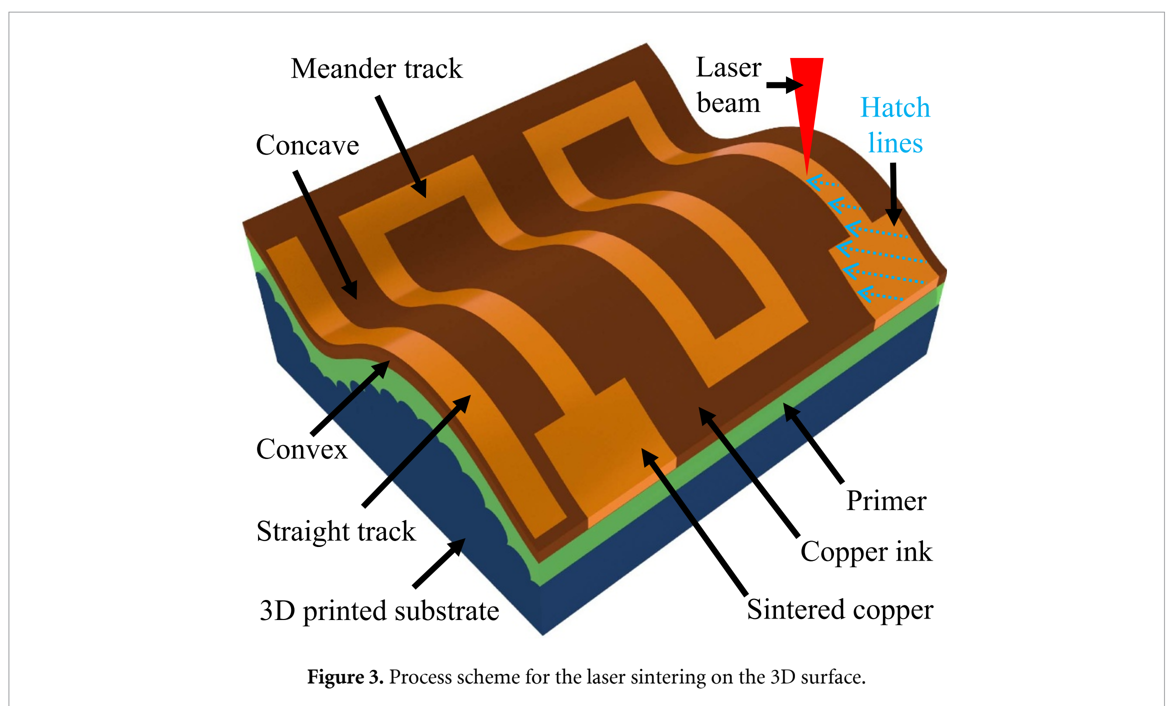

Figure 3. Process scheme for the laser sintering on the 3D surface.

primer provides a uniform surface roughness and fills the pores. The copper ink (DM-CUI-5002, Dycotec Materials Ltd [17]) is applied on top of the cured primer by dip-coating. The primer-coated substrate dips in the copper ink bath twice before starting the drying process to ensure a homogeneous ink layer. A heat gun at 50 °C and 300 l min^{-1} dries the ink for about 5 min. The copper ink coating and drying process steps repeat twice to avoid any defects and obtain sufficient ink layer thickness for the sintering

Table 2. EDXS analysis of material composition.

Process parameters		Measurement results	
Power in W	I_P in W mm^{-2}	Resistance in Ω cm^{-1}	Copper in atom %
0.20	32.1	2.63 ± 0.30	75.0 ± 5.0
0.30	48.1	2.17 ± 0.08	89.9 ± 1.0
0.34	54.5	2.45 ± 0.20	84.1 ± 1.5

process. The final step producing conductive copper traces on additive manufactured 3D surfaces is the sintering process with an 'ns pulsed' 3D laser scanner system (LPKF 160i). The laser system has the following general parameters: 1.064 nm (Nd:YAG), 100 kHz pulse frequency, 65 μm beam focus, 1.3 beam quality factor (M^2) and +4 mm defocusing (resulting in a 126 μm beam spot diameter with an area of 1.2×10^{-2} mm^2). The experiments parametrize the laser power with a fixed laser spot feed rate of 40 mm s^{-1} and a hatch distance (space between the sequential laser processing lines) of 65 μm, which results in approximately 46% of beam overlap. It ensures that summarized intensity fluctuations related to the Gaussian beam shape are less than 5% of the peak intensity ($I_P = 2 \times \text{power} \times \text{area}^{-1}$). A 65° hatch angle enables better compatibility to the meander shape structure. The sintered structures (straight track for parametrization or meanders for validation) always include 45° sidewall surfaces and rounded areas (convex and concave). The laser beam projection to the 45° sidewalls leads to fluctuation of the effective intensity and hatch distance, as already introduced by Overmeyer *et al* [18]. At the 45° sidewalls, the intensity reduces up to 30% compared to the (convex or concave) area due to higher projected elliptical beam area ($126 \times 126\ \mu\text{m} \times \cos(45°)^{-1} \times \pi = 1.7 \times 10^{-2}$ mm^2). This effective intensity fluctuation needs particular consideration when evaluating the results. The 46% beam overlap ratio is independent of the 3D projection because of the increasing hatch distance with $\cos(45°)^{-1}$ on the 45° sidewalls.

3. Results

3.1. Leveling of surface

The initial surface roughness of the investigated substrates is mainly higher than 1 μm for Ra and higher than 10 μm for Rz, as shown in table 2. When pre-treated with primer, the surface shows a reduced roughness of less than 100 nm for Ra and less than 1 μm for Rz. It follows the thesis that the primer creates a uniform leveled surface. The cross-sectional views of processed samples from different substrates in figure 4 prove the primer's flat leveling.

These images clarify the importance of pre-treatment with the primer. It creates a uniform and homogeneous substrate surface, enabling a successful conductor generation process. The FDM substrate has exceptionally high Rz values, while on the MJM substrate, we observe overhangs that would break any thin conducting structure on top of it. The overhangs from the MJM substrate result from the surface connection to supporting material during the additive manufacturing process. SLA surfaces also contain visible steps and defects, while SLS substrates have large pores. Consequently, these substrates will suck up the copper ink if no primer pre-treatment is applied. After primer pre-treatment, the components have similar surface properties, which separates the substrate's 3D printing from the subsequent trace generation process.

3.2. Laser sintering

The laser parametrization in this paper uses statistical analyses to determine the straight tracks' minimum resistance value on a 3D-surface. The sintering of six straight 300 μm wide tracks for every laser parameter combination on a wave-shaped 3D substrate with a rounding radius of 3 mm proofs the result. The power values range between 0.22 W and 0.44 W in increments of 0.02 W. The corresponding peak intensity fluctuates during the process due to the change in spot size. Figure 5 presents the two-point resistance measurement results of this parametrization.

All measurement series result in a bathtub curve and prove that the pre-treatment works. However, the curve is not the same for all components. Since the primer roughness is the same for all samples, the substrate-specific absorption characteristics could probably induce smaller processing windows. A higher laser absorption leads to more heat agglomeration and causes thermal-induced cracks in the conductive trace or even a copper ablation. This theory goes well with the experimental observation that the photopolymer from the MJM samples has a relatively high transmissivity for the 1.064 nm laser radiation. Additionally, various coefficients of thermal expansion mismatch between the different substrate materials and the epoxy primer could explain the smaller processing windows for SLA and FDM substrates. However, power values in the range of 0.3–0.32 W are optimal (small resistances and standard deviations) for all substrates. For most processes (except SLA), a more extended power range from 0.26 to 0.32 W results in low resistances. On MJM and SLS substrates, sintered tracks exhibit conductivity up to 0.4 W. Compared to the results of the single beam sintering of Zenou *et al* [11], despite hatching, the obtained process window peak intensities in this study (27.22–54.5 W mm^{-2}) are in the same order of magnitude. The wide tolerance enables to sinter more complex circuit shape, like meanders. In figure 6, a picture obtained with focus stacking shows a meander shaped sintered structure.

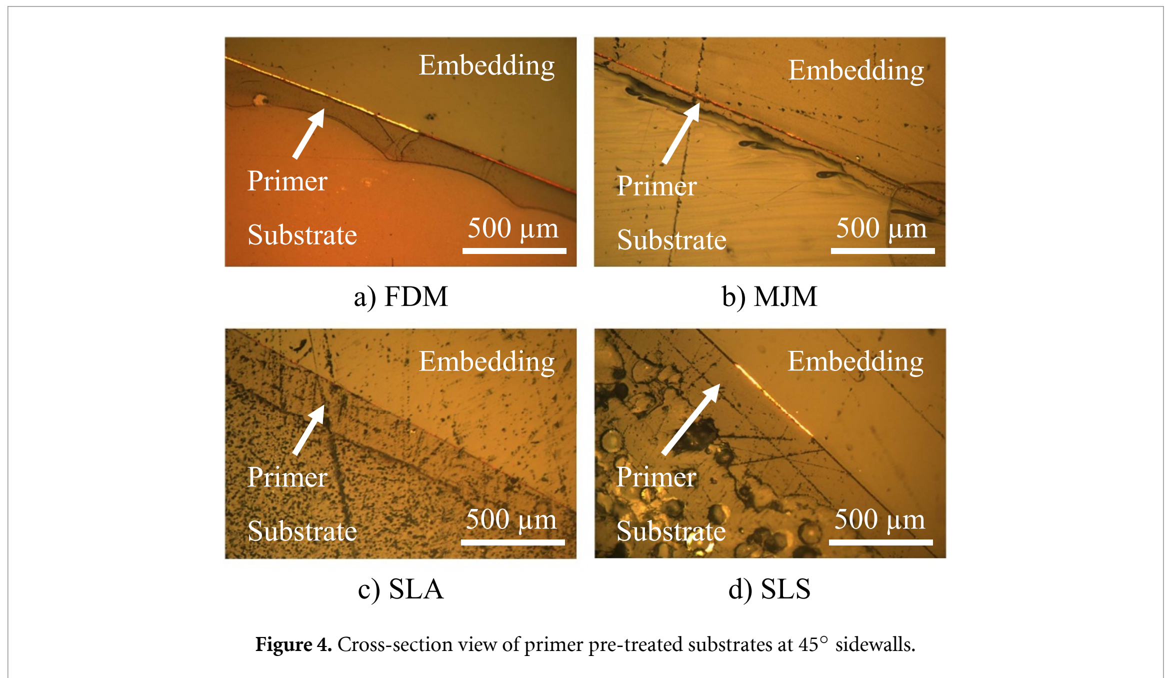

Figure 4. Cross-section view of primer pre-treated substrates at 45° sidewalls.

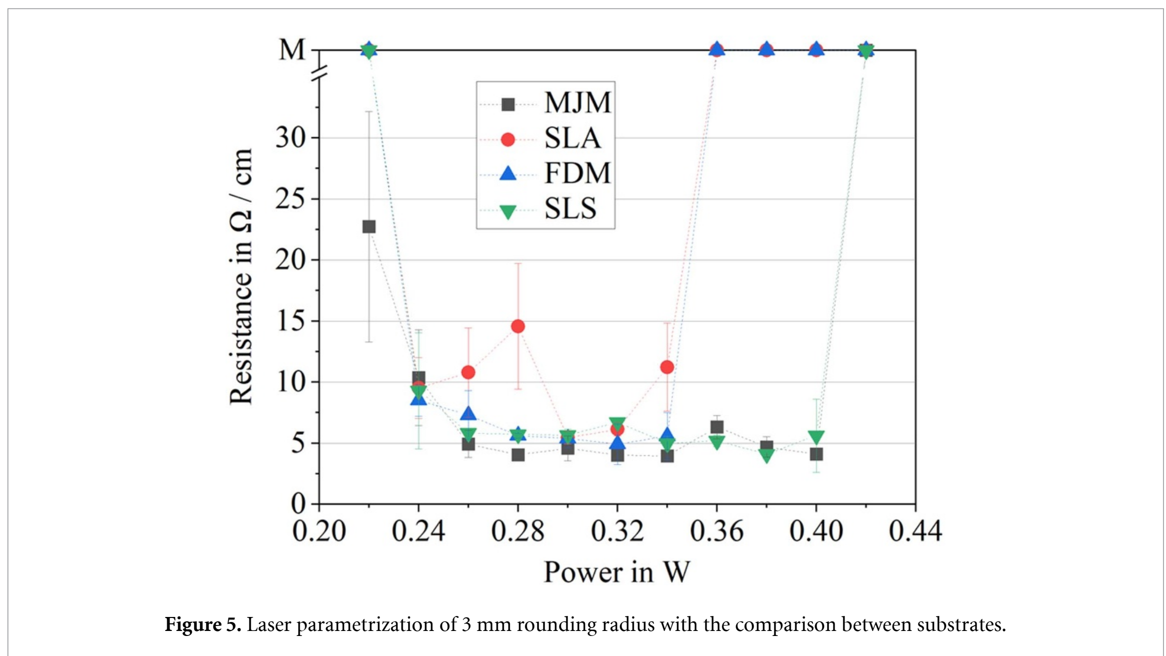

Figure 5. Laser parametrization of 3 mm rounding radius with the comparison between substrates.

The measured resistance corresponds to the 4 Ω cm^{-1} of 0.28 W straight tracks from the parametrization measurements in figure 5. The meanders on the rounding with 1 mm and 3 mm radius also work! Depending on the rounding radius, the resistance varies by $\pm$15 Ω. Relatively low power of 0.28 W (max peak intensity 44.9 W mm^{-2}; min peak intensity 31.8 W mm^{-2}) from the process window enables the successful 3D sintering of the contact pads and the tracks. A higher laser power leads to overheating of the 1 mm^2 contact pads due to larger heat agglomeration. It follows that the effect of heat agglomeration influences the optimal structuring results additionally. In figure 7, a microscope image (3D focus stacked) shows the top view of the previously shown meander laser sintering result in detail.

The accumulation of vertical glossy stripes in the area of the roundings results from the illumination. Several dark spots are visible on the meander's right side, resulting from excess ink during the coating and drying process. A negative influence on the conductance is not noticeable, which indicates a thicker conductive trace at the dark spot areas. In contrast, too thin ink layers tend to burn at high amounts of heat. Comparing the brightness at the rounded areas and the 45° sidewalls make the peak intensity fluctuations visible. The lower the

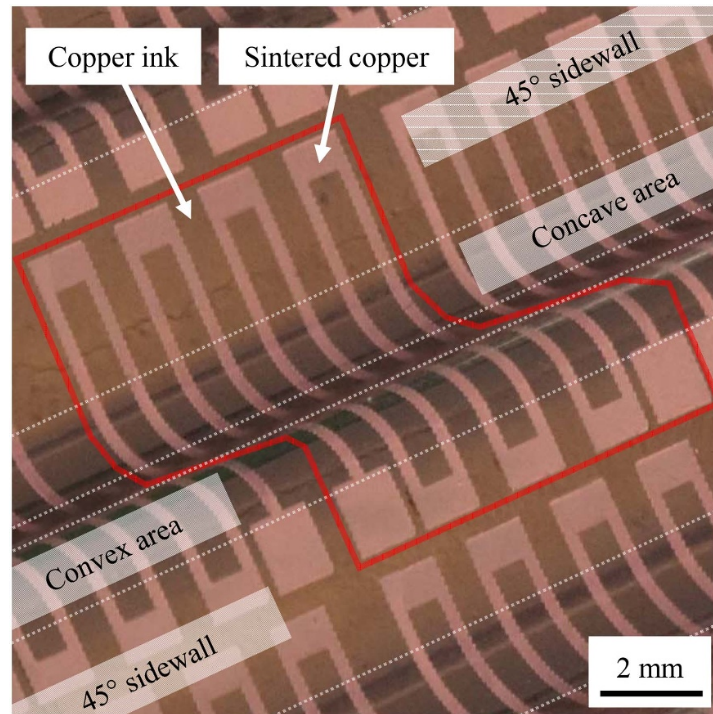

Figure 6. Laser sintered meander (0.28 W) on SLA substrate with 72 Ω resistance.

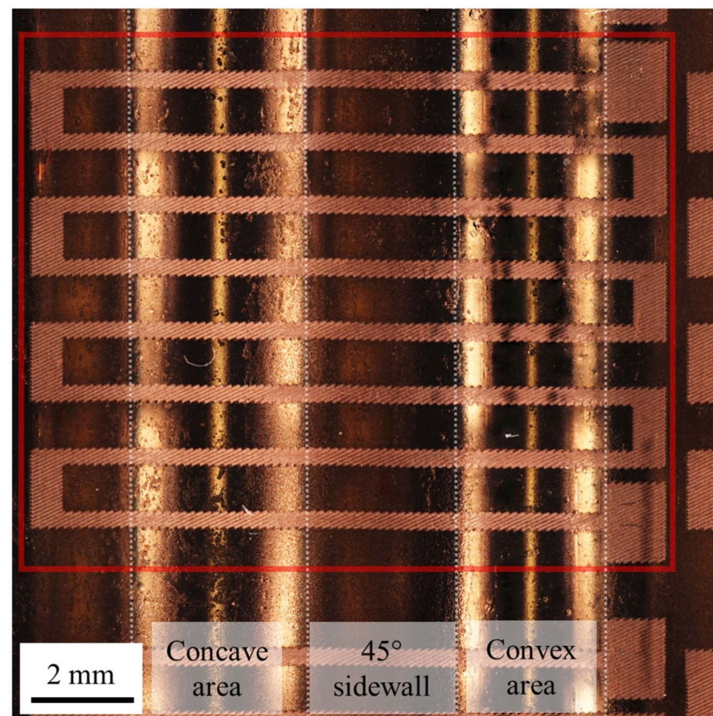

Figure 7. Details of laser-sintered meander (0.28 W) on SLA substrate with 72 Ω resistance.

intensity is, the darker the sintered traces become. This effect appears on the 45° sidewalls, where the peak intensity is only 70% of its maximum value. On the rounding, the beam area is smaller, resulting in higher peak intensity and brighter traces.

3.3. Specific resistivity

It is only possible to determine a top limit for the specific resistivity because the 3D sintered conductive trace consists of an in-homogenous phase. Hatching with the laser beam results in repeating patterns with inhomogeneous material composition. The laser

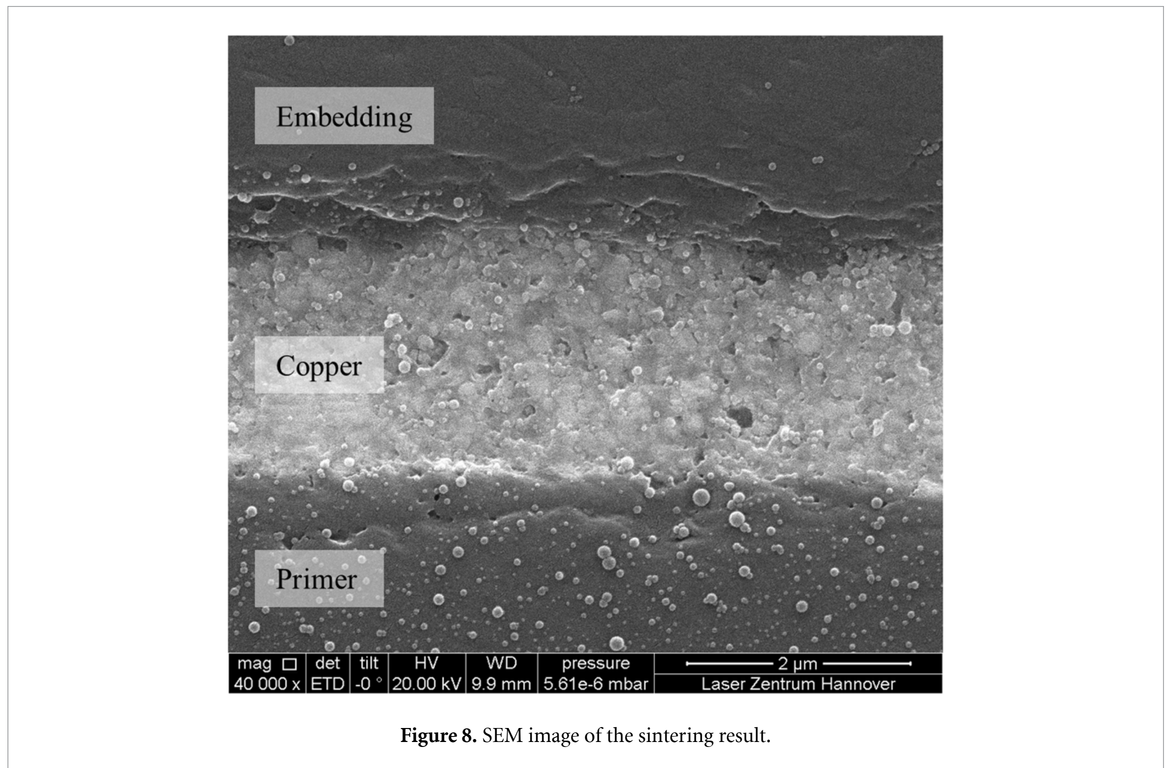

Figure 8. SEM image of the sintering result.

treats the structuring areas with either the inner or outer of the Gaussian intensity distribution. Simultaneously, the 46% overlapping ratio results in areas with a single (8%) and double (92%) laser exposure. Furthermore, the 3D geometry-induced intensity fluctuations lead to different sintering behavior and varying specific resistivity on the sidewalls and rounded areas. Additionally, the wetting of the 3D surfaces is not 100% uniform. Concave areas collect more ink than convex regions due to surface tension effects, which results in the inhomogeneous thickness of the coating and conductive trace. These factors lead to slight changes in the properties along the tracks. The total resistivity determines by the points with the worst properties. Consequently, some areas of the 3D conductive trace show an even lower value than the measured resistivity. Cross-section imaging with a scanning electron microscope (SEM) visualizes the exact trace thickness. Figure 8 contains a representative picture.

The mean conductor thickness in this measurement series is 2 μm. Consequently, the cross-sectional area is 600 μm^2. The minimal measured resistance in the laser parametrization is 4 Ω cm^{-1}. The contact resistance from the two-point measurement is about 2 Ω. Taking this into consideration, a resistivity of about 12 $\mu\Omega$cm is realistic. This value is close to the manufacturer's information of copper ink (8.7 $\mu\Omega$ cm) and well below ten times the value of elemental copper (1.8 $\mu\Omega$ cm).

3.4. Material analyses

The material analysis experiments focus on 2D MJM samples with a primer pre-treatment to study the laser peak intensity's effect on the resulting cross-section. A four-point measurement setup determines the corresponding resistances before the embedding and polishing of the cross-section views. Figure 9 contains three cross-sectional views resulting from low, medium and high sintering power.

On the right side of the three pictures, un-sintered ink is visible. In figure 9(a), the low intensity leads to periodic dark areas with a hatch distance of 65 μm, which indicate partially sintered structures resulting in low conductance. This intensity corresponds to the minimal intensity occurring during the meander sintering (figures 6–7) and shows the expectable sintering result at the 45° sidewalls. Figure 9(b) presents a well-sintered conductor resulting from the meanders rounded areas corresponding intensity. Figure 9(c) shows the effect of higher increased laser sintering power. A rising number of thermal stress cracks is visible with the increase of intensity. Table 2 shows the corresponding atom percentage obtained by EDXS measurement for each sample from figure 9.

Due to the partially sintered areas in figure 9(a), the EDXS measurements' fluctuation ($n = 9$ with 10 μm distance) is much higher. The results correlate with the measured resistance values. Low resistance values match with high copper content and vice versa.

3.5. Assembly with SMD components

Compared to previous tests, the primer pre-treatment shows much better adhesion overall. For example, the test needles used in resistance measurements do not destroy the contact pads while measuring. As seen on the contact pads in figure 7, resistance measurement results in small scratches only. That is a

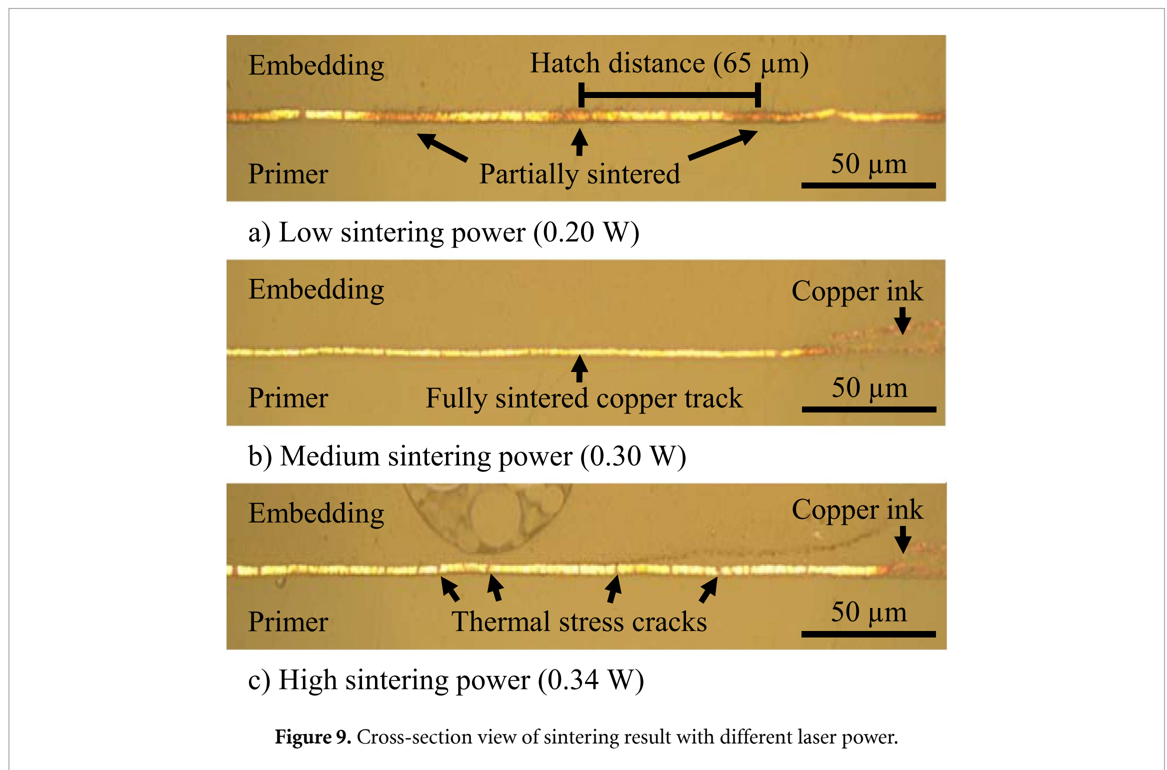

Figure 9. Cross-section view of sintering result with different laser power.

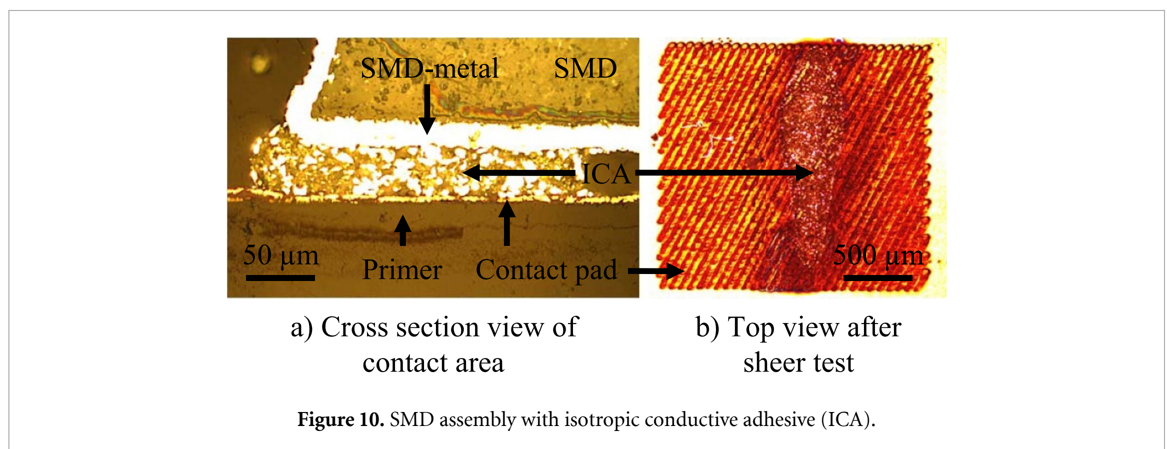

Figure 10. SMD assembly with isotropic conductive adhesive (ICA).

considerable improvement compared to the sintering of conductive traces without a primer pre-treatment or unsuitable primer materials tested in this study's preliminary work. Investigating the assembly with SMD resistors by isotropic conductive adhesive (ICA) (Delo Dualbond® IC343, dried at RT) shows promising results in shear tests. The maximum measured shear strength ranges between 4.8 MPa and 6.6 MPa. After the shear test, the contact pad is intact, and only the ICA breaks, as shown in figure 10. These results give the first idea for a possible assembly process of the conductive traces on primer pre-treated 3D-surfaces.

3.6. Electric tests

3D MJM primer pre-treated substrates with approximately 4 cm long straight tracks determine the maximum current values the conductive traces can withstand. The tracks pass across the entire substrate (figure 1), including six rounded areas (three convex and three concaves) with three different radii (1 mm, 2 mm and 3 mm) and seven 45° sidewall surfaces in total. The analysis evaluates three tracks with initial close resistances. In the experiment, the voltage increases by 300 mV steps (5 s hold) starting from 0V. The resistance calculates from the mean current values and the voltage. Figure 11 shows the mean resistant increase for conductive traces sintered with the same laser power values as in the power parametrization processing window from figure 5.

The standard deviation for the current is smaller than 10 mA, while the standard deviation for the resistances is smaller than 2 Ω cm^{-1} for the complete data. The predominant linear increase in resistance results from the temperature increase by Joule heating. For the trace geometries under investigation, 10 mA corresponds to a current density of approximately 16 A mm^{-2}. Figure 12 shows the

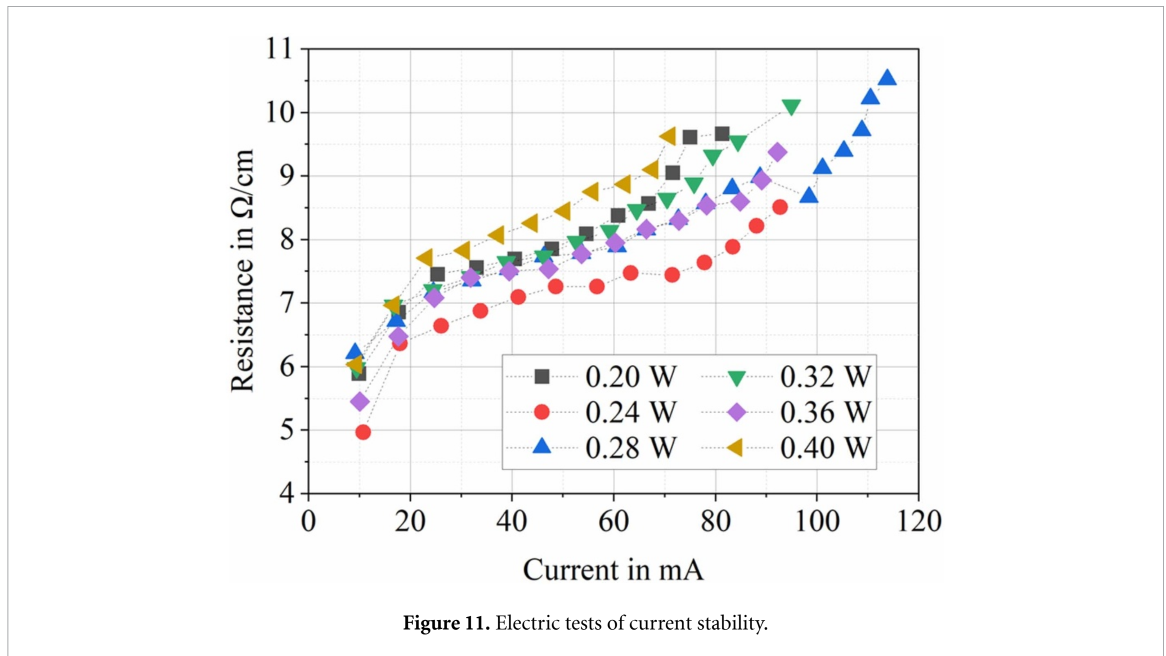

Figure 11. Electric tests of current stability.

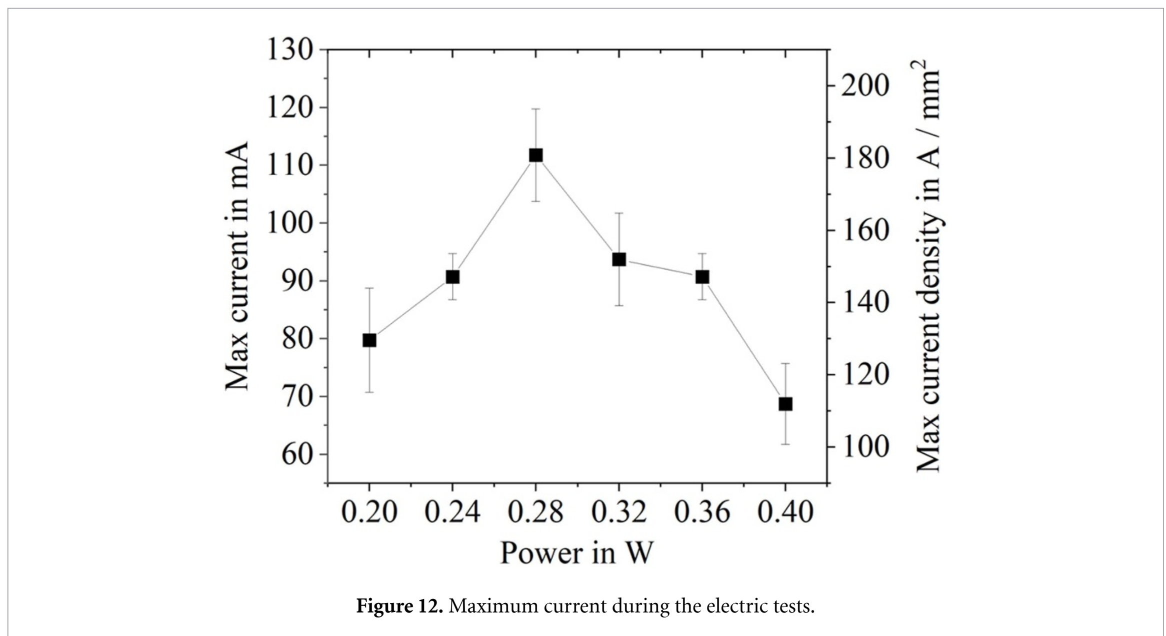

Figure 12. Maximum current during the electric tests.

maximum current and current densities as a function of the laser power.

The data correlate with the bathtub graphs in figure 5. The middle of the processing window (0.24–0.32 W) provides the highest current densities. Destructive overheating at the maximum currents mostly occurs close to the convex rounded areas with a 1 mm radius. That is due to the surface tension at the convex 1 mm rounded areas results in the thinnest ink coating, which minimizes the tracks' cross-sectional area at these points and thus locally causes the highest current density. An additional effect observed during the tests is the decrease of the initial resistance when the test aborts before the tracks' destruction. That indicates that electric post-curing occurs that can be used for thermal sintering as well [19]. A breakdown voltage test measures the un-sintered ink's dielectric strength. The voltage increases between two closely spaced contact pads up to 40 V until the breakdown occurs. Only contact pads with a gap smaller than 20 μm showed a short circuit, indicating that the un-sintered ink's breakdown voltage between the contact pads is higher than 2 kV mm^{-1}. In another experiment, two closely spaced test needles on the primer coating surface determine the primer material's dielectric strength with the same breakdown voltage measurements. These experiments indicate a dielectric strength of more than 10 kV mm^{-1} for the primer material, ensuring good insulation between the substrate and the conductive traces. Thereby the primer pre-treatment enables the processing of laser-sintered conductive traces on conductive substrate materials as well.

4. Conclusion and outlook

This paper introduces a new manufacturing approach for conductive trace manufacturing with printed electronics techniques on additive manufactured substrates with 3D surfaces. It consists of dip-coating methods to apply the primer and a low viscose copper ink and consecutive laser sintering with hatching for the conductive trace generation. The primer pre-treatment provides the opportunity to produce conductive tracks on any additive manufactured substrate. The pre-treatment solves the primary initial problems of additive manufactured substrates such as roughness, porosity and thermal stability. The laser sintering parametrization gives a wide process window on all investigated substrates. Detailed microscope images show that the decreased intensity due to the beam projection on the 45° sidewalls locally decreases the sintering efficiency. Nevertheless, by choosing suitable parameters from the process window, the process enables low resistance 3D meander circuits.
Most important findings:

(a) Primer roughness Ra < 100 nm and Rz < 1 μm
(b) Specific resistivity < 18 $\mu\Omega$ cm
(c) Copper material percentage > 90 atom %
(d) Maximum current densities > 100 A mm^{-2}
(e) Lateral breakdown voltages $>$ 2kV mm^{-1}

However, quantitative adhesion strength measurements are necessary to understand the compatibility better to further processes. Therefore, detailed investigation and further improvement of adhesion would be the main focus of future work. Nevertheless, the findings already represent important prerequisites for a future application of the technology on 3D free-form surfaces. Based on this, a more detailed investigation of the influence of geometrical factors like radii and sidewall angles is possible. Other primers are available and may be suitable for the leveling process. Furthermore, tests with other low viscosity metal inks combined with the primer pre-treatment could validate the integration of different conductive materials on additive manufactured surfaces.

Acknowledgments

The authors like to thank the German BMWi (Federal Ministry for Economic Affairs and Energy) for funding the project '3D-CopperPrint' project of the AiF (Arbeitsgemeinschaft industrieller Forschungsvereinigungen 'Otto von Guericke' e.V.) within the IGF (Industrielle Gemeinschaftsforschung), with the IGF Project No. 20133 N.

ORCID iDs

Ejvind Olsen https://orcid.org/0000-0002-3043-2627

Ludger Overmeyer https://orcid.org/0000-0002-5356-8463

References

[1] Johnson K, Zemba M, Conner B, Walker J and Cortes P 2019 Digital manufacturing of pathologically-complex 3D printed antennas *IEEE Access* **99** 1
[2] Saada G, Layani M, Chernevousky A and Magdassi S 2017 Hydroprinting conductive patterns onto 3D structures *Adv. Mater. Technol.* **2** 1600289
[3] Kwok S W *et al* 2017 Electrically conductive filament for 3D-printed circuits and sensors *Appl. Mater. Today* **9** 167–75
[4] Guo Y, Patanwala H S, Bognet B and Ma A W K 2017 Inkjet and inkjet-based 3D printing: connecting fluid properties and printing performance *Rapid Prototyping J.* **23** 562–76
[5] Gath C and Drummer D 2016 Circuit board application to additive manufactured components by laser-direct-structuring *2016 12th Int. Congress Molded Interconnect Devices (MID): Scientific Proc.* (*Würzburg, Germany, 28–29 September 2016*) pp 1–6
[6] Sun Y and Niino T 2016 Laser sintering of LDS material *2016 12th Int. Congress Molded Interconnect Devices (MID): Scientific Proc.* (*Würzburg, Germany, 28–29 September 2016*) pp 1–5
[7] Hoerber J, Glasschroeder J, Pfeffer M, Schilp J, Zaeh M and Franke J 2014 Approaches for additive manufacturing of 3D electronic applications *Proc. CIRP* **17** 806–11
[8] Roshanghias A, Krivec M and Baumgart M 2017 Sintering strategies for inkjet printed metallic traces in 3D printed electronics *Flex. Print. Electron.* **2** 45002
[9] Ahmadloo M and Mousavi P 2013 A novel integrated dielectric-and-conductive ink 3D printing technique for fabrication of microwave devices *2013 IEEE MTT-S Int. Microwave Symp. Digest (MTT)* pp 1–3
[10] Goth C, Putzo S and Franke J 2011 Aerosol Jet printing on rapid prototyping materials for fine pitch electronic applications *2011 IEEE 61st Electronic Components and Technology Conf. (ECTC)* (*Lake Buena Vista, FL, USA, May 2011–June 2011*) pp 1211–6
[11] Zenou M, Ermak O, Saar A and Kotler Z 2014 Laser sintering of copper nanoparticles *J. Phys. D: Appl. Phys.* **47** 25501
[12] Yu J H, Kang K-T, Hwang J Y, Lee S-H and Kang H 2014 Rapid sintering of copper nano ink using a laser in air *Int. J. Precis. Eng. Manuf.* **15** 1051–4
[13] Ryu J, Kim H-S and Hahn H T 2011 Reactive sintering of copper nanoparticles using intense pulsed light for printed electronics *J. Elec. Mater.* **40** 42–50
[14] Kwon J *et al* 2016 Low-temperature oxidation-free selective laser sintering of Cu nanoparticle paste on a polymer substrate for the flexible touch panel applications *ACS Appl. Mater. Interfaces* **8** 11575–82
[15] Roy N K, Foong C S and Cullinan M A 2018 Effect of size, morphology, and synthesis method on the thermal and sintering properties of copper nanoparticles for use in microscale additive manufacturing processes *Addit. Manuf.* **21** 17–29
[16] Roy N K *et al* 2017 A comprehensive study of the sintering of copper nanoparticles using femtosecond, nanosecond, and continuous wave lasers *J. Micro Nano-Manuf.* **6** MSEC2017
[17] Dycotec Materials Ltd *Dycotec Materials—Advanced Materials Development* (available at: https://www.dycotecmaterials.com/) (Accessed: 28 June 2020)
[18] Overmeyer L, Duesing J F, Suttmann O and Stute U 2012 Laser patterning of thin film sensors on 3 D surfaces *CIRP Ann.* **61** 215–8
[19] Roberson D A, Wicker R B and Macdonald E 2012 Ohmic curing of printed silver conductive traces *J. Electron. Mater.* **41** 2553–66